Modeling magnetization curves in magnetic thin films with striped patterns

2016 J. Phys.: Condens. Matter 28 136001

(http://iopscience.iop.org/0953-8984/28/13/136001)

IOP Publishing Journal of Physics: Condensed Matter
J. Phys.: Condens. Matter **28** (2016) 136001 (9pp) doi:10.1088/0953-8984/28/13/136001

Modeling magnetization curves in magnetic thin films with striped patterns

M Di Pietro Martínez[1], J Milano[1,2,3], M Eddrief[3,4,5], M Marangolo[3,4,5] and S Bustingorry[2]

[1] Instituto Balseiro, Universidad Nacional de Cuyo, Av. Bustillo 9500, (R8402AGP) San Carlos de Bariloche, RN, Argentina
[2] Consejo Nacional de Investigaciones Científicas y Técnicas, Centro Atómico Bariloche—CNEA, Av. Bustillo 9500, (R8402AGP) San Carlos de Bariloche, RN, Argentina
[3] LIFAN, Laboratorio Internacional Franco-Argentino en Nanociencias
[4] Sorbonne Universités, UPMC Univ Paris 06, UMR 7588, 4 place Jussieu, F-75005, Paris, France
[5] CNRS, UMR 7588, Institut des Nanosciences de Paris, 4 place Jussieu, F-75005, Paris, France

E-mail: sbusting@cab.cnea.gov.ar

Received 11 November 2015, revised 28 January 2016
Accepted for publication 29 January 2016
Published 4 March 2016

Abstract

In this work, we study magnetic thin films presenting magnetic stripe patterns. A fingerprint of such domains is a linear behavior of the in-plane magnetization curves below a given saturation field. We present free energy models for the in-plane magnetization curves which permit us to extract key geometrical information about the stripe patterns, such as the maximum canted angle of the magnetization and the domain wall width. As an example, we discuss in this work magnetization curves for $Fe_{1-x}Ga_x$ magnetic films which present a stripe pattern with a period of 160 nm and we found a typical maximum canted angle of 85° and a domain wall width around 30 nm.

Keywords: magnetic thin films, magnetic patterns, magnetostrictive materials, magnetic free energy models

(Some figures may appear in colour only in the online journal)

1. Introduction

There exists a large number of physical and chemical systems which display domain patterns. Some interesting examples are mesoscopic structures formed by assembling polymers in solution or other complex fluids [1, 2], domain structures in magnetic systems [3, 4], or patterning in surface deposition [5, 6]. A key ingredient accompanying pattern formation is the existence of at least two competing interactions acting at different length scales [7].

In the particular case of magnetic systems, domain and pattern formation have attracted much interest since its understanding can be crucial for many technological applications. When considering magnetic systems, the competition between short range exchange interaction, which promotes homogeneous magnetic configurations at small length scales, and the unavoidable long-range dipolar interaction, which favors inhomogeneous configurations at large length scales, is primarily responsible for pattern formation. One of the simplest situations one might consider is a quasi two-dimensional system with strong out-of-plane anisotropy. In this case, one commonly observed pattern is the stripe pattern where an alternating out-of-plane magnetization is formed [8, 9], as observed for example in magnetic garnets [10–12] and thin magnetic films [13–15].

In order to discuss some interesting features presented in these systems, lets consider $Fe_{1-x}Ga_x$ thin films as a concrete example (to be further considered along this work). The inset of figure 1 shows a magnetic force microscopy (MFM) image of a $Fe_{0.8}Ga_{0.2}$ sample with a nominal thickness of 70 nm measured at room temperature in a remnant state [16]. The MFM signal can be related to the out-of-plane magnetization (due to the magnetic interaction between the MFM tip and the stray field gradient generated by the sample magnetization), then this technique is particularly useful to observe the stripe domains. As can be observed, the stripes are oriented in

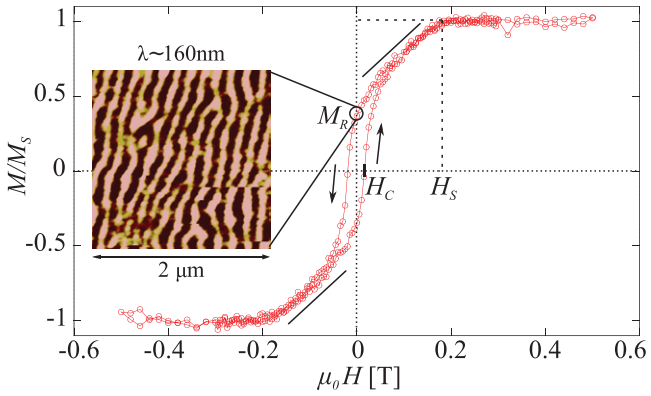

Figure 1. In-plane magnetic cycle at room temperature for a $Fe_{0.8}Ga_{0.2}$ sample with a nominal thickness of 70 nm. The straight lines show the linear behavior which is a distinctive feature of samples with stripe domain patterns. Inset: The out-of-plane magnetization component measured with magnetic force microscopy at room temperature for the same sample in remnant state. The coercive field H_C, the saturation field H_S and the remnant magnetization M_R are also indicated.

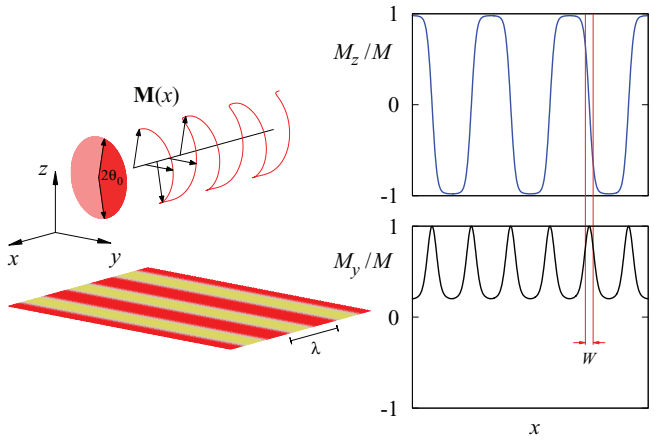

Figure 2. A simplified image of the striped magnetic domains in the form of a canted magnetization state. The left figure shows the rotation of the magnetization vector $\mathbf{M}(x)$ along the x axis and the stripe signal proportional to the M_z component. The right figures show how the out-of-plane (upper panel) and in-plane (lower panel) components of the magnetization change along the x direction. Note that while M_z/M can only take values between $\pm\sin\theta_0$, M_y/M takes its maximum value of 1 at the center of the domain wall and its minimum value of $\cos\theta_0 > 0$ at the core of the stripe domains. The key geometrical parameters are identified: the stripe period λ, the maximum canted angle θ_0, and the domain wall width W.

a preferred direction, which can be controlled during stripes formation under an in-plane applied magnetic field. As shown in the main panel of figure 1, when a large in-plane magnetic field is applied, the magnetization is fully aligned with the field and the sample is then in an homogeneous in-plane magnetic state. When the magnetic field is reduced, the stripe pattern becomes stable at a finite magnetic field, given rise to a decrease of the in-plane magnetization and the characteristic linear behavior shown in figure 1. In fact, this observed linear behavior is a signature of the presence of stripe domain patterns in in-plane magnetic measurements. Finally, the orientation of the stripe pattern corresponds to the direction of the last visited homogeneous in-plane saturation magnetic state, a phenomenon known as rotatable anisotropy [8, 17, 18].

Some salient features about the in-plane hysteresis magnetic cycle shown in figure 1 can be noticed. Firstly, the coercive field H_C is indicative of the energy cost associated to the mechanism of inversion of the in-plane magnetization. Secondly, the saturation field H_S corresponds to the in-plane external field necessary to reach an homogeneous in-plane magnetic state. The saturation field is expected to be proportional to an effective magnetic anisotropy K^{eff} and inversely proportional to the saturation magnetization, $H_S = 2K^{\text{eff}}/M_S$. Finally, when the external magnetic field is removed, there exists a remnant magnetization value M_R indicating that the stripe pattern is composed not only of an alternating out-of-plane magnetization but it also contains a finite in-plane contribution. This suggests to rationalize the stripe pattern in the simple geometrical model described in figure 2. This canted magnetic model shows a magnetization distribution with finite projections onto both out-of-plane and in-plane directions, with the stripe array having a period λ as indicated. Moreover, two further features characterize the stripe pattern within this model: the maximum canted angle θ_0 between the local magnetization direction and the plane of the sample and the domain wall width W separating two stripe domains with opposite homogeneous magnetization.

In this work, in order to obtain quantitative results from the in-plane magnetization curves of magnetic thin films presenting stripe patterns, we present a free energy model based on a canted magnetization configuration, as the one presented in figure 2. As a concrete example we shall focus on the in-plane magnetization curves of two $Fe_{1-x}Ga_x$ thin magnetic samples. We will show that the free energy model permits us to characterize in detail the inner structure of the stripe domains, providing values for the period of the stripe pattern, the maximum canted angle, the domain wall width and the effective change in the magnetostatic energy, all parameters related to the inhomogeneous distribution of the magnetization. The rest of the work is organized as follows: section 2 presents experimental details of the used samples. The free energy model is presented in section 3 while the analysis of in-plane magnetization curves and main results are contained in section 4. Finally, section 5 is devoted to the conclusions of the present work.

2. Experimental

In the following, we shall present experimental information about the studied samples. We will focus on sample growth, structural and magnetic characterization, and the determination of relevant physical parameters, such as the saturation magnetization and the perpendicular magnetic anisotropy.

2.1. Sample growth and structural characterization

Epitaxial $Fe_{1-x}Ga_x$ samples were grown by molecular beam epitaxy on c(2 × 2) Zn-terminated ZnSe epilayers onto GaAs(1 0 0) substrates [19, 20]. At the end, the films were

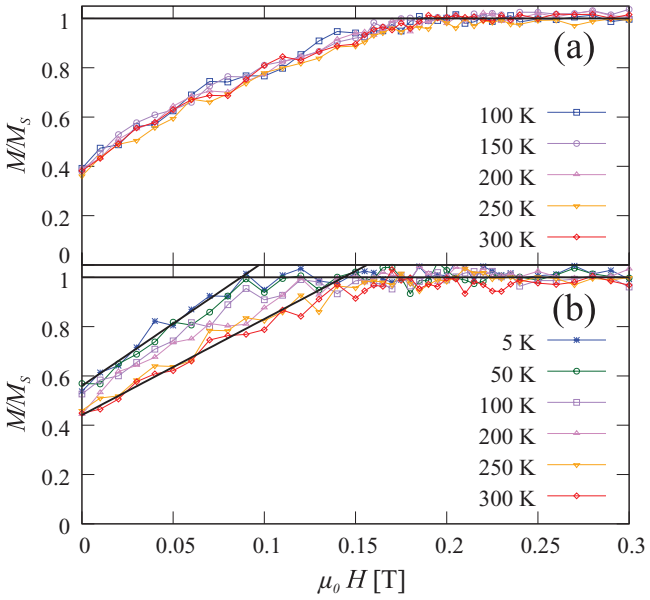

Figure 3. In-plane magnetization curves, M/M_S versus H, for (a) $x = 0.20$ and (b) $x = 0.16$ samples at different temperatures as indicated. Black lines in (b) correspond to linear fits for the 5 K and 300 K data. In both figures the relative error is smaller than 10%.

covered by a protective 3 nm gold capping layer. Details of the growth are given in [21]. We fabricated 70 nm nominal thick samples at two Ga concentration values, $x = 0.16$ and 0.20. Such concentrations were determined by means of x-ray photoelectron spectroscopy (XPS) and confirmed by Rutherford backscattering (RBS) and energy dispersive x-ray spectrometry (EDX). The $x = 0.16$ sample was annealed at 300°C in ultra high vacuum [21]. This annealing temperature is sufficient to cause Ga mobility in the Fe matrix, as attested in [22] and, at the same time, it preserves the sharp ferromagnetic/semiconductor interface [19]. By x-ray diffraction (XRD), we determine the lattice parameters and we observe the Ga dependent tetragonal deformation in the as-grown samples and the recovered cubic structure due to annealing [21].

2.2. Magnetic characterization

2.2.1. In-plane magnetization curves. The characteristic in-plane magnetization curves, M versus H, were measured using a vibrating sample magnetometer (VSM) and a superconducting quantum interference device (SQUID). For all measurements, the external magnetic field was applied in the plane of the samples (in-plane configuration). It is important to mention that M versus H curves present an isotropic behavior in the film plane, since we obtain the same result when curves are taken at different crystallographic directions. In addition, since we are interested in the linear behavior and its relation with the stripe pattern, the M versus H curves were only taken from a starting field of 1 T down to reach zero applied field. For each sample, in-plane magnetization curves were taken at several temperatures in the range 5 K $< T <$ 300 K. A diamagnetic contribution due to the sample holder was subtracted and the curves were normalized to the saturation value M_S in all cases. In figures 3(a) and (b), we show the M versus H curves at several

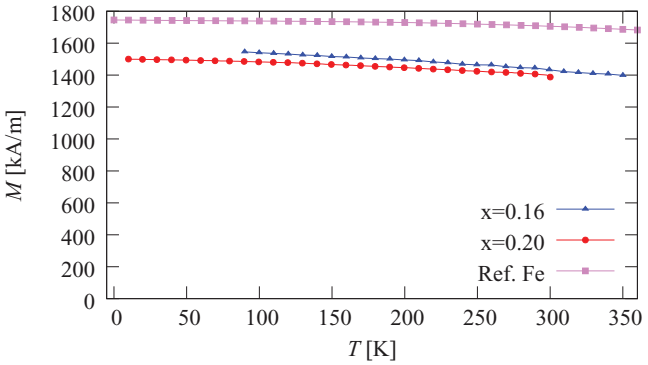

Figure 4. Temperature dependence of the saturation magnetization M_S for the studied samples, as indicated in the key. The saturation magnetization of Fe is included as a reference value.

temperatures for the $x = 0.20$ and annealed $x = 0.16$ samples respectively. Both samples present the typical response of the magnetic system where stripe domains are present as we stated in the Introduction, i.e. a linear dependence of $M(H)$ is observed for H values lower than the saturation field, H_S. However, the evolution of such linear behavior with temperature depends on the sample. For the $x = 0.20$ sample (see figure 3(a)) there is not a significant difference between curves at different temperatures, i.e. the saturation field, H_S, and the magnetization remanence, M_R, do not depend on temperature. On the other hand, for the $x = 0.16$ sample (figure 3(b)), the M versus H curves show a clear dependence with temperature, with H_S (M_S) increasing (decreasing) for higher temperatures. For example, black lines in figure 3(b) are linear fits performed for the 5 K and 300 K curves, and using the intersection between those lines and the $M/M_S = 1$ constant, it is found that the saturation field rises from about 900 G to 1600 G when the temperature increases from 5 K to 300 K.

2.2.2. Determination of M_S and K_n. The key parameters governing the appearance and behavior of the stripe patterns are the saturation magnetization, M_S, and the perpendicular magnetic anisotropy, K_n, as it is explicitly shown in the free energy models discussed in section 3. For obtaining M_S, SQUID magnetization curves as a function of temperature were performed from 5 K to 300 K in the saturation state (no stripes present) at 0.2 T in both samples as it is shown in figure 4.

In order to study K_n in our samples through ferromagnetic resonance (FMR), we have to evaluate how the magnetic anisotropies present in the sample contribute to the resonance field, H_r. We then propose a self-consistent scheme that solves the equilibrium position of the magnetization vector $\mathbf{M}_S$ via the magnetic free energy density U and a linearized version of the Landau–Ginzburg equation of motion for the magnetization [23], when the sample is magnetically saturated. Hence, the proposed expression for U in our coordinate system (figure 5(a)) is the following:

$$U(\vartheta,\varphi) = -\mu_0 \mathbf{H}_{\text{app}} \cdot \mathbf{M}_S + \frac{\mu_0}{2} M_S^2 \cos^2\vartheta + K_n \cos^2\vartheta + K_u \sin^2\vartheta \cos^2\left(\varphi - \frac{\pi}{4}\right) + U_{\text{MCA}} \quad (1)$$

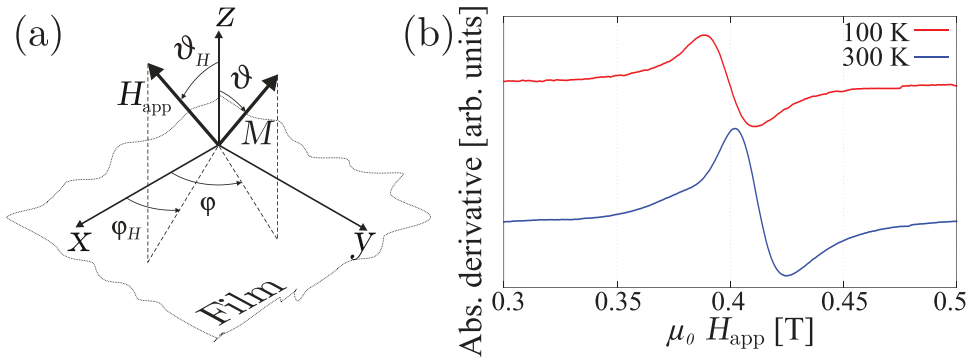

Figure 5. (a) Coordinate system used in our calculations to extract magnetic anisotropies. (b) FMR spectra taken at 100 K and 300 K for the $x = 0.20$ sample and for the external field H_{app} applied in the [1 0 0] direction.

Table 1. M_S, K_n, K_u, K_4 and K_4^{tet} values experimentally obtained at 100 K and 300 K for both studied samples.

Sample	T [K]	M_S [kA m^{-1}]	K_n [$\times 10^5$ J m^{-3}]	$K_4(K_4^{tet})$ [$\times 10^4$ J m^{-3}]	K_u [$\times 10^3$ J m^{-3}]
$x = 0.20$	100	1500 ± 200	3.35 ± 0.05	1.7 ± 0.1	4 ± 1
$x = 0.20$	300	1400 ± 200	3.43 ± 0.05	0.5 ± 0.1	4 ± 1
$x = 0.16$	100	1500 ± 200	3.85 ± 0.05	1.9 ± 0.1	2 ± 1
$x = 0.16$	300	1400 ± 200	3.70 ± 0.05	0.9 ± 0.1	2 ± 1

Note: K_4 and K_4^{tet} stand for the fourfold in-plane anisotropy of $x = 0.16$ and 0.20 respectively.

where $\mathbf{H}_{app}$ is the applied magnetic field and μ_0 is the vacuum permeability ($\mu_0 = 4\pi \times 10^{-7}$ T m A^{-1}). The first term on the right-hand side is the classical Zeeman energy. The second one is the energy related to the demagnetizing dipolar field. The third term is the energy related to the perpendicular magnetic anisotropy K_n, including the out-of-plane magnetic anisotropy K^{OP} coming from magneto-crystalline effects [24] as discussed below when referring to U_{MCA}. The fourth one stands for an uniaxial in-plane anisotropy arising from the $Fe_{1-x}Ga_x$/ZnSe interface [25, 26]. Finally, the fifth term is related to the magnetocrystalline anisotropy (MCA) contribution to the magnetic free energy, and thus U_{MCA} depends on the crystal symmetry of the sample under study. On one hand the $x = 0.16$ sample presents a cubic structure due to the annealing procedure. Then, for this sample

$$U_{MCA} = \frac{1}{4} K_4 (\sin^2 2\vartheta + \sin^4 \vartheta \sin^2 2\varphi), \qquad (2)$$

which is the usual expression for cubic lattices at first order [27]. On the other hand, it is important to notice that the tetragonal distortion along z-axis that suffers the $x = 0.20$ sample, as mentioned in section 2.1, modifies the cubic anisotropy energy term given in equation (2). As a result, the cubic term $[K_4^{cub}(\alpha_x^2\alpha_y^2 + \alpha_y^2\alpha_z^2 + \alpha_z^2\alpha_x^2)]$ becomes now $K_4^{tet}\alpha_x^2\alpha_y^2 + K^{OP}\alpha_z^2$, where the out-of-plane α_z^4-term was neglected in our calculations. α_i denotes the direction cosines of the magnetization which, using the coordinate system shown in figure 5(a), are defined as $\alpha_x = \sin\vartheta\cos\varphi$, $\alpha_y = \sin\vartheta\sin\varphi$ and $\alpha_z = \cos\vartheta$. Then, for the $x = 0.20$ sample the magnetocrystalline contribution writes:

$$U_{MCA} = \frac{1}{4} K_4^{tet} \sin^4\vartheta \sin^2 2\varphi, \qquad (3)$$

while the out-of-plane contribution $K^{OP}\alpha_z^2$ effectively enters into the perpendicular magnetic anisotropy K_n.

The equation that accounts for the magnetization dynamics in the small oscillation approximation was given by Smit and Beljers [23] and it writes:

$$\omega^2 = \frac{\gamma^2}{M_S^2 \sin^2\vartheta} \left[\frac{\partial^2 U}{\partial^2\vartheta} \frac{\partial^2 U}{\partial^2\varphi} - \left(\frac{\partial^2 U}{\partial\vartheta\partial\varphi} \right)^2 \right] \Bigg|_{\vartheta_{eq},\varphi_{eq}}, \qquad (4)$$

evaluated at the equilibrium angles, ϑ_{eq} and φ_{eq} obtained from equation (1), where $\gamma = g\mu_B/\hbar$ is the gyromagnetic ratio and μ_B is the Bohr magneton. The g value was set to 2.1, as for Fe.

As an example, figure 5(b) presents FMR spectra at two different temperatures for the $x = 0.20$ sample. The shift between such spectra is due to the change of magnetization and magnetic anisotropy with temperature.

In table 1 we summarize the values of M_S and K_n at $T = 100$ K and 300 K for both samples. Besides, a typical value for the stiffness constant in $Fe_{1-x}Ga_x$ samples, $A = 1.6\,10^{-11}$ J m^{-1}, was considered [28]. These parameters will be taken as input values when using free energy models to quantify the inner structure of stripe patterns in the following section. The other fitting parameters (K_4^{tet}, K_4, K_u) are also given in table 1. Note that in spite of having in-plane anisotropies (K_4^{tet}, K_4, K_u), the hysteresis loops are isotropic in the film plane, as we stated previously, since when the magnetization distribution is not homogeneous (for $H < H_S$) the perpendicular magnetic anisotropy and dipolar terms dominate over in-plane magnetic anisotropies.

3. Modeling magnetization curves

In order to analyze magnetization curves, we introduce in this section a free energy model based in a canted domain structure

such as the one schematized in figure 2. Within this model, we consider an array of parallel straight stripes oriented along the y-direction and whose position dependent magnetization is

$$\mathbf{M} = M_S(0, \cos\theta(x), \sin\theta(x)), \tag{5}$$

meaning that the magnetization is always oriented along the longitudinal direction of the stripes. The angle $\theta(x)$ is the angle between $\mathbf{M}$ and the x-y plane, i.e. the surface of the sample, and depends only on the transverse direction of the stripe pattern. Notice that, on one hand, since we are considering an array of parallel straight stripes the magnetization is homogeneous along the y-direction, and on the other hand, while $M_x = 0$, the components $M_y = M_S \cos\theta(x)$ and $M_z = M_S \sin\theta(x)$ change along the x-direction as shown in figure 2. In this situation the profile of the position dependent magnetization is thus defined through the one-dimensional angle profile $\theta(x)$ along the transverse direction of the stripe pattern.

We propose to work with the following free energy density model, which contains the relevant energy contributions to be considered:

$$f[\theta(x)] = -\mu_0 H M_S \cos\theta(x) + \frac{1}{2}\mu_0 M_S^2 (1 - E_{dip}) \sin^2\theta(x) + K_n \cos^2\theta(x) + A\left(\frac{\partial\theta(x)}{\partial x}\right)^2. \tag{6}$$

The first term corresponds to the Zeeman energy with $\mathbf{H} = H\hat{y}$, so that this term is minimized when the magnetization is fully in-plane in the field direction, i.e. $\theta(x) = 0$. The second energy contribution is the one corresponding to the stray field, or so-called demagnetizing energy. When $E_{dip} = 0$ and considering an homogeneous solution $\theta(x) = \bar{\theta}$, the stray field of a thin magnetic film is minimized when all the magnetization lies on the plane, i.e. $\bar{\theta} = 0$. When the magnetization is inhomogeneous the stray field can be computed only in very special cases of $\theta(x)$. Therefore we consider here a generic correction factor E_{dip} taking into account how much the stray field departs from the homogeneous thin film case when a general $\theta(x)$ is used. The factor E_{dip} thus gives not only information about the changes in the stray field induced by the stripe pattern, but it also absorbs any other dipolar magnetic contribution not considered in the canted model, as for example the one coming from closure domains close to thin film surfaces. The third term is the anisotropy energy contribution controlled by the perpendicular magnetic anisotropy constant K_n. When $K_n > 0$, this energy term is minimum for an homogeneous magnetization aligned perpendicular to the surface, i.e. $\theta(x) = \bar{\theta} = \pm\pi/2$. Therefore, one can link the competition between the stray field and the perpendicular magnetic anisotropy to the presence of inhomogeneous solutions as the stripe pattern. A common measure of this competition is given by the quality factor $Q = K_n/(1/2\,\mu_0 M_S^2)$; with $Q > 1$ ($Q < 1$) indicating that the system is unlikely (likely) to present stripe patterns with a canted magnetization distribution [3]. Finally, the last term in equation (6) is the exchange interaction term and corresponds to the energy density cost associated to spatial variations of the magnetization, controlled by the stiffness constant A. This exchange term is then minimized whenever the magnetization is homogeneous, i.e. $\theta(x) = \bar{\theta}$. The energy cost of a domain wall between up and down magnetization regions can be estimated by considering anisotropy and exchange terms, giving a domain wall energy of order $4t\sqrt{AK_n}$, where t is the thickness of the sample, and an associated domain wall width W of order $\sqrt{A/K_n}$ [3]. It is important to note that this last model does not include the in plane anisotropies, i.e. K_4, K_4^{tet}, K_u because of the fact that the M versus H curves are isotropic in the film plane. Also, it is worth stressing at this point that the simplified model we are using, based on the one-dimensional magnetization profile defined in equation (5), does not allow to model the formation of closure domains. However, in [29], it is explicitly shown that for $Q < 0.4$, as is the case for the $Fe_{1-x}Ga_x$ samples analyzed here [16], one-dimensional models (if compared with those where closure domains are taken into account, as in [9]) give a good description of the magnetostatic energy when stripes are present.

The starting point in order to extract some information from the experimental magnetization curves is a trial angle profile $\theta(x)$. Given a proposed model for the angle profile $\theta(x)$ the free energy model, equation (6), is used to compute the average energy contained within a stripe, defined through the stripe free energy density

$$F = \frac{1}{\lambda}\int_0^{\lambda} dx\, f(\theta(x)), \tag{7}$$

obtained by integrating over the period of the stripe pattern, λ. Since the system is periodic, the full free energy for a finite size system can be written in terms of F. The stripe free energy density depends on material parameters (M_S, K_n and A) and on geometrical information of the stripe pattern distribution such as its period λ, the domain wall width W and the maximum canted angle θ_0, all contained in the angle profile $\theta(x)$. For the material parameters M_S, K_n and A we use experimental determined values, as presented in section 2. Then, for given trial values for E_{dip} and λ, the normalized in-plane magnetization $M_y(H)/M_S = \cos\theta(H)$ is computed by minimizing the stripe free energy density F with respect to the angle profile-dependent geometrical parameters for each value of H. Finally, the values for E_{dip} and λ are varied to get the best agreement between the predicted $M_y(H)$ and the experimental data.

The domain wall width can be defined in several ways and we shall use here two options. One in terms of the tangent of the magnetization angle, considering the intersection of the tangent line passing through the middle of the domain wall where $\theta = 0$ and the constant value corresponding to the magnetization angle limit inside the stripe domains where $\theta = \theta_0$, i.e. $\theta_0' \times (\Delta/2) = \theta_0$, where θ_0' is the slope at the middle of the domain wall. Therefore, the domain wall width would be

$$\Delta = \frac{2\theta_0}{\theta_0'}. \tag{8}$$

A second definition can be obtained with the same idea but using instead the out-of-plane magnetization, i.e. through the

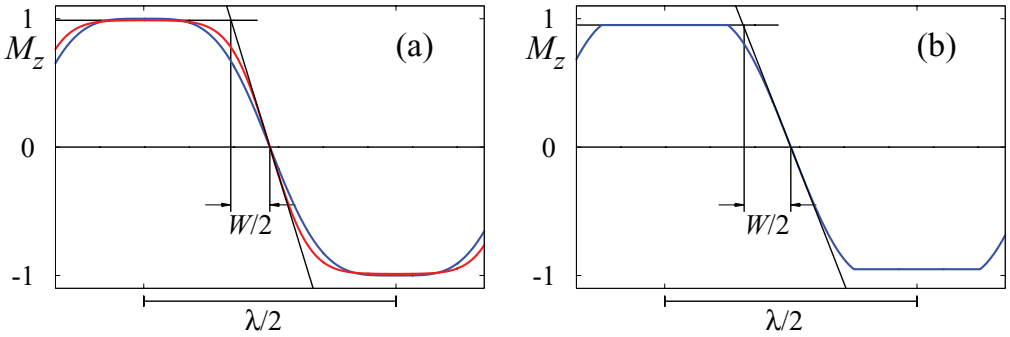

Figure 6. Out-of-plane magnetization component $M_z(x)$ corresponding to the (a) cosine series expansion and (b) the trapezoidal model. In (a) one-mode and two-mode approximations are shown in blue and red curves respectively. The geometrical construction used to compute the domain wall width W is shown for each model (in (a) only for the two-mode profile).

tangent of the out-of-plane magnetization at the middle of the wall and the intersection with the out-of-plane magnetization within the stripe domain, as shown in figure 6. This results in $\partial_x M_z(\theta = 0)(W/2) = M_z(\theta = \theta_0)$, where $M_z(\theta = \theta_0)$ is the out-of-plane magnetization within the stripe domain. Therefore,

$$W = \frac{2M_z(\theta = \theta_0)}{\partial_x M_z(\theta = 0)}. \tag{9}$$

In fact, since $M_z = M_S \sin(\theta)$, both definitions are related through

$$W = \Delta \frac{\sin(\theta_0)}{\theta_0}. \tag{10}$$

A typical order of magnitude for a 180° domain wall between two semi-infinite domains is $W = \sqrt{A/K_n}$. Finally, although Δ is appropriate to deal with angle profile models, we shall use W to compare between the different cases below. In general, the domain wall width W depends on the materials parameters and on the profile model properties, as discussed below for each particular case.

In the following, and in order to fit the experimental data using the free energy model, we shall consider two angle profile models which permit us to study and compare different limits of the relation between domain wall width and stripe period: a cosine series expansion (small λ/Δ) and a trapezoidal model (large λ/Δ).

3.1. Cosine series expansion

Considering the limit in which the domain wall width and the extent of the domain itself are of the same order, the angle profile can be thought as a simple cosine expansion of the form

$$\theta(x) = \theta_1 \cos(kx) + \theta_2 \cos(3kx) + \theta_3 \cos(5kx) + \ldots \tag{11}$$

where θ_n is the amplitude of the nth-order term and $k = \frac{2\pi}{\lambda}$, which then enforces the profile $\theta(x)$ to have a period λ. In the following, we shall refer to the n-mode cosine expansion when truncating the expansion up to nth-order. Using this angle profile, the stripe free energy density defined through equation (7) is computed. In the particular 1-mode case the following closed expression is found:

$$F = -HM_S J_0(\theta_1) + \frac{1}{4}\mu_0 M_S^2 (1 - E_{dip})\,[1 - J_0(2\theta_1)] + \frac{K_n}{2}\,[1 + J_0(2\theta_1)] + \frac{2A\pi^2\theta_1^2}{\lambda^2}. \tag{12}$$

where $J_0(x)$ is the 0th-order Bessel function of the first kind. For $n > 1$ the integral definition for F is numerically computed. For the given values of λ and E_{dip}, the minimization of F with respect to the θ_n's for each H value gives the $M(H)$ curve. In this work we shall consider the stripe free energy density up to 3rd-order of the cosine expansion in order to take into account different shapes of the profile. Notice that in the limit of very large n, the profile defined by the cosine expansion tends to a square wave stripe pattern.

For the cosine expansion proposed here, the maximum canted angle is $\theta_0 = \sum_n \theta_n$, and using the definition for the domain wall width, equation (9), we obtain

$$W = \frac{\lambda}{\pi} \frac{\sin\left(\sum_n \theta_n\right)}{\sum_n (-1)^n (2n+1)\theta_n}, \tag{13}$$

which permits us to have a measure of the domain wall width in terms of the stripe period and the modes amplitudes.

Figure 6(a) shows the out-of-plane magnetization profile $M_z(x)$ corresponding to the cosine series expansion with one- and two-modes. The geometrical construction to compute the domain wall width W is also indicated (see equation (9)).

3.2. Trapezoidal stripe domain

We consider here the limit in which the domain region defining the stripes is much larger than the finite domain wall separating these regions (similarly to the model proposed in [30] to study stripped thin films at remanence). In this limit the magnetization is perfectly homogeneous within the domain while all the spatially varying magnetization is restricted to the domain wall region. Furthermore, we consider a linear variation of the angle profile within the domain wall. Therefore, the model angle profile can be considered to be a stepwise function with constant values $\pm\theta_0$ within the stripe domains while linear ramps with slopes $\pm\theta_0'$ are connecting these domains. In this case, the extent of the ramped region is exactly the domain wall width in terms of the angle profile, $\Delta = 2\theta_0/\theta_0'$.

Choosing an arbitrary origin for the stripe pattern, the angle profile can be written in terms of θ_0 and Δ as

$$\theta(x) = \begin{cases} -\theta_0 & \text{for} \quad 0 \leqslant x < \lambda/2 - \Delta, \\ 2\theta_0/\Delta\,[x - (\lambda/2 - \Delta/2)] & \text{for} \quad \lambda/2 - \Delta \leqslant x < \lambda/2, \\ \theta_0 & \text{for} \quad \lambda/2 \leqslant x < \lambda - \Delta, \\ -2\theta_0/\Delta\,[x - (\lambda - \Delta/2)] & \text{for} \quad \lambda - \Delta \leqslant x < \lambda. \end{cases} \tag{14}$$

Using this model for the angle profile, with parameters θ_0 and Δ, the stripe free energy density can be split into two parts,

$$F = \left(1 - \frac{2\Delta}{\lambda}\right) f(\theta_0) + \frac{2\Delta}{\lambda} g(\theta_0, \Delta), \tag{15}$$

with $2\Delta = 4\theta_0/\theta_0'$ thus representing the linear extension of the two ramp regions defined in the trapezoidal angle profile, equation (14). Therefore the stripe free energy density is composed of the free energy density within the domain regions, given by

$$f(\theta_0) = -HM_S\cos(\theta_0) + \frac{1}{2}\mu_0 M_S^2(1 - E_{\text{dip}})\sin^2(\theta_0) + K_n\cos^2(\theta_0) \tag{16}$$

and the domain wall free energy density, given by

$$g(\theta_0, \Delta) = \frac{1}{2\theta_0}\Big[-2HM_S\sin(\theta_0) + \frac{1}{2}\mu_0 M_S^2(1 - E_{\text{dip}})(\theta_0 - \cos(\theta_0)\sin(\theta_0)) + K_n(\theta_0 + \cos(\theta_0)\sin(\theta_0))\Big] + A\left(\frac{2\theta_0}{\Delta}\right)^2. \tag{17}$$

Using this model, the two parameters θ_0 and Δ are obtained in the minimization process.

Finally, the domain wall W is given by equation (10) in terms of θ_0 and Δ. Figure 6(b) presents the out-of-plane magnetization profile $M_z(x)$ resulting from the ramped angle profile $\theta(x)$ of equation (14) together with the geometrical construction to compute the domain wall width W.

4. Results and discussion

Using the proposed profiles described in the previous section, we intend to reproduce the experimental M versus H curves. Experimental values for K_n, M_S, and A were measured, as described in section 2, and used as input parameters for the profile models. Then, using trial values for λ and E_{dip} the magnetization curves can be constructed by minimizing the free energy models with respect to the geometrical parameters, as discussed in section 3.

Firstly, by scrutinizing the free energy models, we can learn what are the main effects of changing the values of λ and E_{dip}. On one hand, increasing E_{dip} causes the linear zone characteristic of the presence of stripe patterns to move to higher fields, rising the saturation field being the most prominent effect. On the other hand, increasing λ decreases the remanence magnetization while keeping H_S almost constant.

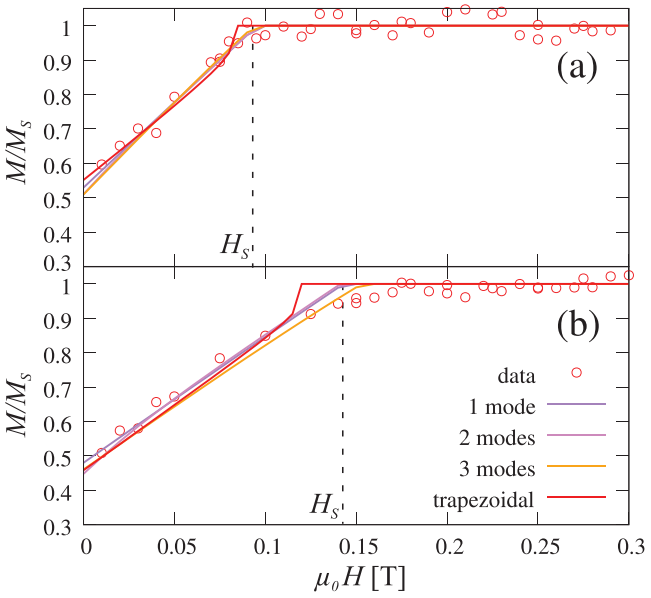

Figure 7. Experimental data for the $x = 0.16$ sample measured with VSM (dots) and results from modeling the magnetization curves (lines) corresponding to the different proposed profiles, as indicated. Results corresponding to two different temperatures are shown: (a) $T = 100$ K and (b) $T = 300$ K.

Table 2. Characteristic values for the $x = 0.16$ sample at 100 K and 300 K obtained using the free energy models, as indicated, and the experimental values for K_n and M_S presented in table 1.

T [K]	Profile	λ [nm]	E_{dip}	θ_0 [°]	W [nm]
100	1 mode	164(10)	0.80(3)	85(3)	34.8(2)
	2 modes	164(10)	0.80(3)	80(3)	28.8(2)
	3 modes	160(15)	0.80(3)	79(3)	26.2(2)
	Trapezoid	120(10)	0.79(3)	56(8)	8.8(2)
300	1 mode	164(10)	0.81(3)	91(3)	32.9(2)
	2 modes	160(10)	0.81(3)	80(3)	21.2(2)
	3 modes	148(10)	0.81(3)	82(3)	22.1(2)
	Trapezoid	160(10)	0.79(3)	63(8)	10.5(2)

Note: The values for θ_0 and W correspond to the remnant state at $H = 0$.

Since both parameters have different marked consequences in the computed magnetization curves, it is safe to search independent values for E_{dip} and λ such that the $M(H)$ curves fit best with the experimental results.

We consider both models, the cosine expansion (up to 3rd-order) and the trapezoidal model, to analyze the experimental data for the $x = 0.20$ and 0.16 samples at $T = 100$ K and 300 K. As an output of the fitting procedure we report for each case λ, E_{dip}, W and θ_0.

In figure 7 we present the experimental data for the magnetization curves corresponding to the annealed $x = 0.16$ sample at 100 K and 300 K, together with the curves corresponding to the cosine series expansion (up to $n = 3$) and trapezoidal models. The obtained parameters are reproduced in table 2. A few facts can be remarked about these results. The trapezoidal model does not correctly capture the appearance of the linear ramp, showing a rather abrupt jump. The value of the stripe period generally agrees with the one obtained from

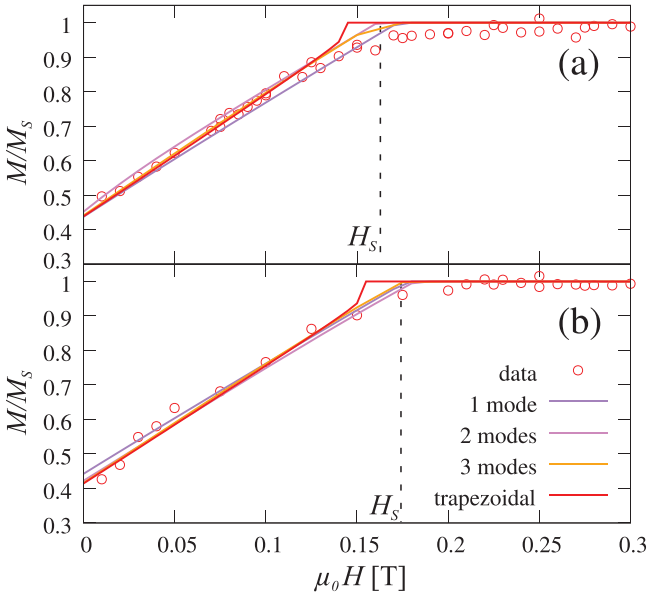

Figure 8. Experimental data for the $x = 0.20$ sample measured with VSM (dots) and results from modeling the magnetization curves (lines) corresponding to the different proposed profiles, as indicated. Results corresponding to two different temperatures are shown: (a) $T = 100$ K and (b) $T = 300$ K.

the MFM images, $\lambda = 160$ nm [16], although the value obtained using the trapezoidal model is slightly smaller for $T = 100$ K. The value of $E_{\rm dip}$ is close to 0.8, which means that the demagnetizing energy is around 20% of the one corresponding to a fully in-plane magnetized thin film. The largest values for θ_0 are obtained for the 1-mode cosine expansion and is typically around 80°, except for the trapezoidal model which has a smaller value close to $\theta_0 = 60°$. The value of the domain wall width W is also reported and it is around 30 nm for the cosine expansion model, but around 10 nm for the trapezoidal model. Over all, cosine expansion models give a more consistent description of the experimental data. Therefore, although $W \approx 30$ nm is larger than the simple estimate $\sqrt{A/K_n} \approx 6.5$ nm, it is a more realistic estimation of the domain wall width.

Finally, the most important difference between the data at 100 K and 300 K is that for the $x = 0.16$ sample the saturation field H_S is smaller for $T = 100$ K, as mentioned in section 2. However, there are no appreciable changes neither in $E_{\rm dip}$, which would strongly modify H_S, nor in the rest of the parameters shown in table 2. This indicates that the stripe profiles are not noticeably changing with temperature while H_S is. Therefore, in fact, the increase in H_S cannot be associated to changes in the stripe pattern and it is only caused by the expected change due to a decrease of the magnetization M_S when the temperature is increased, $H_S \sim 2K^{\rm eff}/M_S$, with $K^{\rm eff}$ an effective anisotropy constant.

Figure 8 shows the experimental data for the $x = 0.20$ sample at $T = 100$ K and 300 K and the corresponding magnetization curves obtained using the free energy models presented in section 3. The resulting parameters are presented in table 3. The stripe period λ agrees with $\lambda = 180$ nm, as measured using MFM images [16, 31], for the 1-mode cosine

Table 3. Characteristic values for the $x = 0.20$ sample at 100 K and 300 K obtained using the free energy models, as indicated, and the experimental values for K_n and M_S presented in table 1.

T [K]	Profile	λ [nm]	$E_{\rm dip}$	θ_0 [°]	W [nm]
100	1 mode	170(10)	0.87(3)	93(3)	33.1(2)
	2 modes	148(10)	0.88(3)	83(3)	21.7(2)
	3 modes	152(10)	0.87(3)	85(3)	20.6(2)
	Trapezoid	100(10)	0.85(3)	64(8)	7.3(2)
300	1 mode	170(10)	0.84(3)	93(3)	33.3(2)
	2 modes	148(10)	0.84(3)	83(3)	22.0(2)
	3 modes	152(10)	0.84(3)	84(3)	21.0(2)
	Trapezoid	140(10)	0.83(3)	65(8)	11.8(2)

Note: The values for θ_0 and W correspond to the remnant state at $H = 0$.

expansion and it is smaller for the other models. $E_{\rm dip}$ is in general a bit larger than for $x = 0.16$, indicating that the stray field energy is even smaller, and θ_0 is of the same order as for $x = 0.16$. The domain wall width is estimated to be close to 25 nm.

Remarkably, unlike the results presented in figure 7 for $x = 0.16$, there is no noticeable change in the saturation field H_S when the temperature is modified, as also shown in figures 3 and 8. However, since the saturation magnetization M_S is decreasing with T (as much as for the $x = 0.16$ sample) an increase of H_S with temperature would be expected. The small decrease of $E_{\rm dip}$ from 0.86 at 100 K to 0.84 at 300 K is indeed responsible for a drop in H_S which compensates the increase expected due to a diminution of M_S with T, thus indicating that in this case a change on the magnetic structure of the stripe pattern can strongly influence the expected magnetization behavior.

5. Conclusions

In summary, we have developed here free energy models which permit us to analyze in-plane magnetization curves of thin films presenting stripe patterns. The free energy model is based on a canted magnetic state and allows to quantify geometrical characteristics of the pattern, such as the stripe period, the maximum canted angle and the domain wall width, together with an estimation of the change of the demagnetizing energy. As an example, we have developed and applied a fitting procedure using these models to analyze measured in-plane magnetization curves for two $Fe_{1-x}Ga_x$ samples which present different temperature behaviors. We found a stripe period which compares well with the one obtained from MFM images. More importantly, we report here estimated values for the maximum canted angle, typically around $\theta_0 = 85°$, and the domain wall width, of the order of $W = 30$ nm. These parameters are valuable to complete a geometrical characterization of the stripe patterns and can be useful to complement micromagnetic simulations [31]. Furthermore, when comparing the $x = 0.20$ and $x = 0.16$ samples the main observed difference is that for the former the dipolar contribution quantified by $E_{\rm dip}$ is not changing while for the later it does. Changes in $E_{\rm dip}$ are directly related to changes in the internal magnetic structure of the stripes. Although in principle one could attribute

this difference to structural differences (the $x = 0.20$ sample being tetragonal while the annealed $x = 0.16$ sample is cubic), it is not easy to directly correlate the observed effects with the micro/nano structure of the samples. Specific experiments giving access to the atomic environment, for example those based on synchrotron radiation, are difficult to carry due to the small amount of mass available in a thin film.

We have presented and used here two free energy models: a cosine series expansion (up to 3rd-order) and a trapezoidal model. Although both models give reasonable estimates for the parameters, the trapezoidal model seems to give systematically odd values (larger λ, smaller θ_0 and W). Since the domain wall width is around 30% of the half-period of the stripe pattern, cosine series expansion models are more suitable in the present case. In particular, the simple 1-mode cosine model gives the more consistent results. Conversely, whenever the domain wall width is a very small fraction of the half-period, of the order of a few percent, we expect the trapezoidal model to be more suitable.

It has recently been shown that x-ray magnetic microscopy can be used, through the angular dependence of its magnetic contrast, to quantitatively access the canted angle of the stripe pattern in a ferromagnetic $NdCo_5$ thin film [15]. However, the space resolution in the same experiment ~ 45 nm is not enough to characterize the domain wall width. Here, we present a simpler alternative which, based on free energy models and the described fitting procedure, permits us to obtain geometrical parameters characterizing stripe patterns, such as the canted angle and the domain wall width, directly from in-plane magnetic measurements.

Acknowledgments

This work was partially supported by ANR (SPINSAW, ANR 13-JS04-0001-01), CONICET (Argentina) through Project PIP11220120100250CO and Universidad Nacional de Cuyo (Argentina) via grant 06/C446.

References

[1] Gelbart W M and Ben-Shaul A 1996 *J. Phys. Chem.* **100** 13169
[2] Bates F S, Hillmyer M A, Lodge T P, Bates C M, Delaney K T and Fredrickson G H 2012 *Science* **336** 434
[3] Hubert A and Schäfer R 2000 *Magnetic Domains* (New York: Springer)
[4] Johansen T H, Pan A V and Galperin Y M 2013 *Phys. Rev.* B **87** 060402
[5] Thyagu N N, Vasilenko A, Voyiadjis A, Glasser B J and Shinbrot T 2012 *Eur. Phys. J.* E **35** 105
[6] Yang S *et al* 2013 *Adv. Funct. Mater.* **23** 720
[7] Seul M and Andelman D 1995 *Science* **267** 476
[8] Lehrer S S 1963 *J. Appl. Phys.* **34** 1207
[9] Murayama Y 1966 *J. Phys. Soc. Japan* **21** 2253
[10] Seul M and Wolfe R 1992 *Phys. Rev.* A **46** 7519
[11] Molho P, Gouzerh J, Levy J and Porteseil J 1986 *J. Magn. Magn. Mater.* **54–7** 857
[12] Molho P, Porteseil J L, Souche Y, Gouzerh J and Levy J C S 1987 *J. Appl. Phys.* **61** 4188
[13] Pappas D P, Kamper K P and Hopster H 1990 *Phys. Rev. Lett.* **64** 3179
[14] Saratz N, Lichtenberger A, Portmann O, Ramsperger U, Vindigni A and Pescia D 2010 *Phys. Rev. Lett.* **104** 077203
[15] Blanco-Roldán C *et al* 2015 *Nat. Commun.* **6** 8196
[16] Barturen M *et al* 2012 *Appl. Phys. Lett.* **101** 092404
[17] Alvarez-Prado L M, Pérez G T, Morales R, Salas F H and Alameda J M 1997 *Phys. Rev.* B **56** 3306
[18] Barturen M, Sacchi M, Eddrieff M, Milano J, Bustingorry S, Popescu H, Jaouen N, Sirotti F and Marangolo M 2013 *Eur. Phys. J.* B **86** 191
[19] Marangolo M, Gustavsson F, Eddrief M, Sainctavit P, Etgens V H, Cros V, Petroff F, George J M, Bencok P and Brookes N B 2002 *Phys. Rev. Lett.* **88** 217202
[20] Eddrief M, Marangolo M, Etgens V H, Ustaze S, Sirotti F, Mulazzi M, Panaccione G, Mosca D H, Lépine B and Schieffer P 2006 *Phys. Rev.* B **73** 115315
[21] Eddrief M, Zheng Y, Hidki S, Salles B R, Milano J, Etgens V H and Marangolo M 2011 *Phys. Rev.* B **84** 161410
[22] Kubaschewski O 1982 *Iron—Binary Phase Diagrams* (New York: Springer)
[23] Smit J and Beljers H 1955 *Philips Res. Rep.* **10** 113
[24] Barturen M, Milano J, Vázquez-Mansilla M, Helman C, Barral M A, Llois A M, Eddrieff M and Marangolo M 2015 *Phys. Rev.* B **92** 054418
[25] Sjöstedt E, Nordström L, Gustavsson F and Eriksson O 2002 *Phys. Rev. Lett.* **89** 267203
[26] Marangolo M *et al* 2004 *Phys. Rev.* B **70** 134404
[27] Cullity B D and Graham C D 2008 *Introduction to Magnetic Materials* (New York: Wiley)
[28] Barturen M 2014 Anisotropía magnética y acople magneto-elástico en películas delgadas de $Fe_{1-x}Ga_x$ crecidas epitaxialmente sobre ZnSe/GaAs(0 0 1) *PhD Thesis* Universidad Nacional de Cuyo and Université Pierre e Marie Curie, Paris VI
[29] Guzmán J, Álvarez N, Salva H, Mansilla M V, Gómez J and Butera A 2013 *J. Magn. Magn. Mater.* **347** 61
[30] Yafet Y and Gyorgy E M 1988 *Phys. Rev.* B **38** 9145
[31] Tacchi S et al *Phys. Rev.* B **89** 024411